# Deep Learning Based High-Resolution Frequency Estimation for Sparse Radar Range Profiles

Sabyasachi Biswas, and Ali C. Gurbuz

Dept. of Electrical and Computer Engineering, Mississippi State University, MS, USA
sb3682@msstate.edu, gurbuz@ece.msstate.edu

Abstract—Frequency estimation is a pivotal process in many signal-processing applications. Generating radar range profiles for linear frequency modulated radar systems is such a case where spectral analysis is used to estimate target ranges. Conventional methods like fast Fourier transform (FFT) are the golden standard in frequency estimation, despite its Rayleigh resolution limit and high sidelobe levels. To address such limitations this paper introduces HRFreqNet; a deep neural network (DNN) architecture for high-resolution frequency estimation from 1D complex time domain data consisting of multiple frequency components. Our deep learning (DL) architecture consists of an auto-encoder block to improve signal-to-noise ratio (SNR), a frequency estimation block to learn frequency transformations to generate pseudo frequency representations(FR), and finally, a 1D-UNET block to reconstruct high-resolution FR. Experimental results on synthetically generated data show enhanced performance in terms of resolution, estimation accuracy, and ability to suppress noise. Achieved range profiles are also sparser with lower sidelobe levels. The proposed HRFreqNet is evaluated over both synthetic and experimental real-world radar data and it is observed that accurate, sparse, high-resolution range profiles are obtained compared to existing approaches.

Index Terms—Stretch processing, Deep Learning, Frequency Estimation, Auto-encoder, Unet, Radar Range profile, Sparsity.

#### I. INTRODUCTION

Frequency estimation of multi-component sinusoidal signals from a finite number of samples is an important problem in signal processing. Frequency estimation is the fundamental element in many applications like radar imaging [1], wireless communication [2], medical imaging [3], audio and speech processing [4], underwater acoustics [5], calibration [6] and many more. For linear frequency modulation (LFM) radar systems, the received signal is dechirped by multiplying it with a local oscillator LFM signal that has the same sweep rate. Distinct targets appear as different frequencies after the mixing operation. To create a radar range profile and estimate the relative ranges of each target, spectrum analysis is applied, and the most commonly used technique for that is the discrete Fourier Transform (DFT). Such spectrum analysis techniques are widely employed for extracting different radar data representations such as range profiles (RP), range-Doppler (RD) representations, range-Angle (RA) domains or micro-Doppler spectrograms ( $\mu$ -DS) [7]. While very few DNN-based architectures use raw radar data directly [8]-[10], one or multiple of these radar data representations have been used in applications like human activity recognition (HAR) [11]-[13], mini-UAV classification [14], indoor monitoring [15], [16], advanced vehicle assistant systems (ADAS) [17], [18], and health monitoring [19].

While the DFT is a powerful tool for frequency estimation, it has certain limitations. When dealing with infinitely long time-domain signals, the DFT can accurately represent the frequency representation (FR) of that signal. However, in real-world applications, signals are finite in length and often corrupted by noise. This finite signal length reduces the resolution of the signal in the frequency domain, consequently affecting the accuracy of frequency estimation. Moreover, high sidelobe levels are observed for DFT and low SNR conditions alleviate the effects of an accurate frequency estimation. To address these challenges, there has been a growing interest in the development of deep learning (DL) based methods for high-resolution frequency estimation. In [20], the authors introduced Deepfreq, a DNN architecture designed to estimate frequencies in a multi-sinusoidal complex-valued signal. This model concatenates the real and imaginary channels, forming a 1D frequency spectrum input for the neural network. In a similar vein, [21] presented Cresfreq, a complex-valued neural network (CVNN) architecture tailored for generating a 1D frequency representation of multi-sinusoidal complexvalued signals. However, these DL methods have drawbacks, including very high computational demands, and sensitivity to noise, limiting their performance at lower SNRs.

Expanding on the insights inspired by Deepfreg, Cresfreg, this paper presents HRFreqNet, a novel end-to-end DNN architecture designed to generate high-resolution FRs from 1D complex-valued signals. The proposed approach offers higher resolution, enhanced noise robustness, and superior computational efficiency. HRFreqNet includes a convolutional auto-encoder for noise reduction, a convolutional frequency estimation block for intermediate frequency representation, and a 1D-UNET block for constructing high-resolution FR. While DFT utilizes sinc function as the basis, which is the reason for both the Rayleigh resolution limit and the sidelobe levels, the proposed approach utilizes a new ground truth labeling structure that leads to higher resolution FR. With the help of the autoencoder and the 1D-UNet blocks, the HRFreqNet can effectively suppress noise, resulting in cleaner and high-resolution FRs using the proposed labels as well as the designed novel weighted loss function scheme. The contributions of this paper can be summarized as follows:

 Development of an end-to-end DNN architecture with a weighted loss function for enhanced noise suppression,

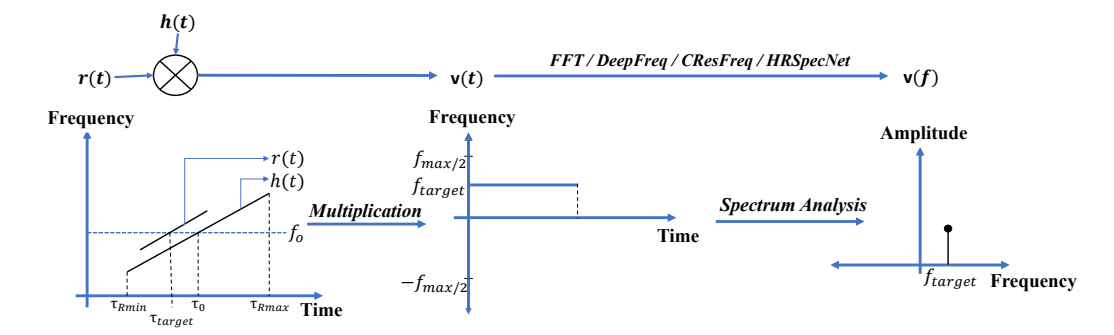


Fig. 1: The SP flow diagram [22]

and generation of accurate and high-resolution frequency representations.

- Investigation of HRFreqNet's advantages over traditional FT, highlighting its cleaner and high-resolution FRs.
- Examples of HRFreqNet's capability to generate sparser radar range profiles from synthetic and real-life raw radar data.

The paper is organized as follows: summarizing the RF signal model for LFM radar systems and existing DL-based spectrum analysis techniques in Section II, discussing HRFreqNet in Section III, analyzing performance in Section IV, and concluding and discussing future directions in Section V.

## II. THEORETICAL BACKGROUND

### A. Radar Signal Model

The radar transmits LFM pulses. This can be modeled as,

$$s(t) = \exp(j\pi\alpha t^2)\operatorname{rect}(\frac{t}{T}),$$
 (1)

$$rect(x) = \begin{cases} 1, & \text{if } |x| < 1\\ 0, & \text{otherwise} \end{cases}$$

where,  $\alpha = \frac{B}{T}$  is the sweep rate, B is the bandwidth and T is the pulse width. If there are M scatterers at ranges  $R_m$ , m = 1, 2, ..., M within the range interval  $[R_{min}, R_{max}]$  around centre range  $R_0$ , the received signal r(t) from all reflectors will be modelled as,

$$r(t) = \sum_{m=1}^{M} A_m \exp(j2\pi f_c(t - \tau_{R_m})) \exp(j\pi\alpha(t - \tau_{R_m})^2),$$
(2)

where,  $f_c$  is the carrier frequency, c is the propagation speed,  $A_m$  is the complex reflectivity and  $\tau_{R_m} = \frac{2R_m}{c}$  is the time delay of the mth scatterer. The time delay w.r.t. the centre range time delay  $\tau_0$  can be written as  $\tau_{R_m} = \tau_0 + \Delta \tau_{R_m}$ .

In stretch processing (SP) using the same sweep rate as s(t), the heterodyne LFM signal can be formulated as,

$$h(t) = \exp(j2\pi f_c(t - \tau_0)) \exp(j\pi\alpha(t - \tau_0)^2),$$
 (3)

resulting in the mixed output which can be written as

$$v(t) = r(t)h^*(t),$$

$$= \sum_{m=1}^{M} \widehat{A_m} \exp(j2\pi\alpha\Delta\tau_{R_m}t) + n(t).$$
(4)

The mixer output, given by the sum of complex exponentials in (3), is affected by additive Gaussian noise n(t), with  $\hat{A}_m$ representing the complex constant terms for the scatterer. The frequency  $f_{R_m}$  of the mth term, corresponding to a relative time delay  $\Delta \tau_{R_m}$ , is expressed as  $f_{R_m} = \alpha \Delta \tau_{R_m}$ . For sampling the mixer output with a lower-rate ADC, the sampling frequency  $F_s$  is determined by the bandwidth in the mixed signal. The signal's bandwidth, arising from a sum of complex exponentials, is linked to the maximum and minimum frequencies dictated by the range window extent. If the time delay interval for the expanded range window is  $\Delta au_{R_m} = au_{R_{max}} - au_{R_{min}}$ , where  $R_{max}$  and  $R_{min}$  are the maximum and minimum time delay values for the corresponding ranges, then the minimum ADC rate  $F_s$  is given by  $F_s = \Delta \tau_{R_{int}}/\alpha$  to be less than the pulse bandwidth B. Uniformly sampling the mixed output at  $F_s$  over the time interval  $\tau_{R_{min}}$   $-\frac{T}{2} \le t \le \tau_{R_{max}} + \frac{T}{2}$  generates at least  $N_s \ge F_s(T + \tau_{R_{int}})$  samples for SP. The target frequencies  $f_{R_m}$ and their corresponding ranges are estimated using traditional DFT or DL-based frequency estimation techniques as shown in Fig. 1. In the subsequent section, we will briefly discuss two existing DL-based estimation techniques: DeepFreq and CresFreq.

## B. DL-based frequency estimation techniques

The DeepFreq framework, introduced in the context of precisely estimating the frequencies of multi-sinusoidal signals from a limited set of noisy samples, utilizes a deep learning-based technique as outlined in [20]. This approach presents a novel DNN architecture that surpasses conventional methods such as DFT in high SNR scenarios. The DeepFreq framework integrates two key modules: one for enhancing frequency representation and another for automatic frequency count estimation within a fixed signal length. While DeepFreq stands as one of the early DL-based methodologies for frequency estimation, it exhibits certain limitations. Notably, its sensitivity to

input signal noise can result in imprecise frequency estimates. Furthermore, the framework lacks the capability to discern the amplitude of individual frequency components within a given signal. Lastly, DeepFreq is characterized by a higher computational complexity when compared to the established DFT approach.

Building upon the foundations laid by DeepFreq, a novel Complex-Valued Neural Network (CVNN), named Cresfreq, has been introduced for high-resolution frequency estimation in 1D complex signals, as detailed in [21]. Cresfreq takes a unique approach by training on complex-valued basis vectors and incorporating convolutional kernels to effectively suppress noise. Real-valued residual blocks are subsequently employed to enhance the resolution of frequency representation. The authors of this paper claim, Cresfreq effectively addresses some of the limitations observed in DeepFreq, particularly in improving performance in low SNR scenarios and providing more accurate estimates of the amplitudes of frequency components. However, it's worth noting that Cresfreq comes with a higher computational latency compared to DeepFreq.

### III. PROPOSED METHOD

This section presents the structure and specifics of our proposed ML approach for frequency estimation. It covers dataset creation, introduces HRFreqNet architecture, and explains the training process with a weighted loss function.

#### A. Dataset Generation

The dataset creation procedure involves two stages. Firstly, we generated multi-sinusoidal 1D complex time-domain signals to serve as inputs for our architecture. Subsequently, we created labeled frequency representations to depict the frequencies of these input signals.

1) 1D Multi-sinusoidal Complex Signal Generation: We utilize multi-sinusoidal signals denoted as s(k) as the dataset inputs. These signals can be represented as,

$$s(k) = \sum_{q=1}^{Q} A_q \exp(j(2\pi f_q k + \theta_q)),$$
 (5)

In the context provided, the component number Q adheres to a discrete uniform distribution  $\mathcal{U}(1,30)$ . The intensity of the qth component, denoted as  $A_q$ , is calculated as  $0.2+2.5|\sigma_q|$ , where  $\sigma_q$  follows a uniform distribution  $\mathcal{U}(0,1)$ . The parameter  $\theta_q$  is drawn from a uniform distribution  $\mathcal{U}(0,2\pi)$ , and the normalized frequency  $f_q$  follows a uniform distribution  $\mathcal{U}(-0.5,0.5)$ . The signal length is K=200 and the minimum separation between two frequencies is 1/N.

2) Ground truth Frequency representations: To generate the ground truth data, first, the whole frequency range (-0.5 to 0.5) is divided into  $N_f=1000$  frequency bins. The initial 1D ground truth  $GT_0(n)$  can be represented as,

$$GT_0(n_f) = \begin{cases} A_q, & (\exists \mathbf{q})(n_f \Delta n_f \le f_q(i) < (n_f + 1)\Delta n_f) \\ 0, & \text{otherwise} \end{cases}$$

where, the frequency index is denoted as  $n_f$  which ranges from 0 to  $N_f-1$ . In this context,  $\Delta n_f=\frac{1}{N_f}$  represents the frequency interval. Afterwards,  $GT_0(n)$  is convolved with a 1D Gaussian kernel with a kernel size of 3 and standard deviation of 0.3/N to generate the final ground truth denoted as  $GT_{final}$ .

## B. Proposed HRSpecNet Architecture

This section introduces HRFregNet, a novel DL architecture designed for high-resolution frequency estimation. Our model comprises three key components: an auto-encoder, a dense layer resembling the DFT, and a 1D U-Net block dedicated to producing high-resolution 1D FRs. The input consists of complex signals with dimensions  $C \times L$ , where C=2 denotes the real and imaginary parts, and L depends on the signal length. During the training process, the network handles noisy signals, with the auto-encoder playing a pivotal role in noise reduction. The output from the auto-encoder is fed into the Fourier transform-like dense layer, responsible for generating multiple proxy FRs. The U-Net block refines these proxies into high-resolution FRs. Throughout the training phase, a weighted loss function is employed, guiding the model to generate high-resolution FRs that closely align with the ground truth while simultaneously mitigating noise present in the input signal. In the subsequent sections, we provide detailed explanations for each block of the HRFregNet architecture.

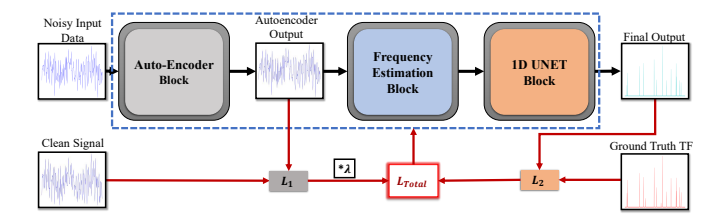


Fig. 2: Flow-diagram of the proposed architecture.

- 1) Auto-Encoder Module: The autoencoder architecture incorporates multiple Conv1D layers aimed at capturing intricate patterns in the input data while simultaneously reducing the feature space dimension. Each Conv1D block is configured with 64 filters, a kernel size of 3, and a stride of 2 for local convolution operations, leading to a reduction in spatial dimensions. This encoding process enables the autoencoder to acquire a concise representation of the input data. The initial input data, shaped as  $2 \times 200$ , is first reshaped into  $1 \times 400$ , with the real part of the signal in the first 200 positions and the imaginary part in the subsequent 200. Throughout the training process, the autoencoder maintains the output shape of  $1 \times 400$ . The model's objective is to minimize the sum of squared error (SSE) loss, denoted as  $L_1$  in Figure 2, by comparing its output to a noise-free version of the input signal. This approach effectively diminishes noise, contributing to the enhancement of the final FR.
- 2) Frequency Estimation Block: The noise-reduced output from the autoencoder block is directly fed into the Frequency Estimation Block. This block employs a dense layer unit

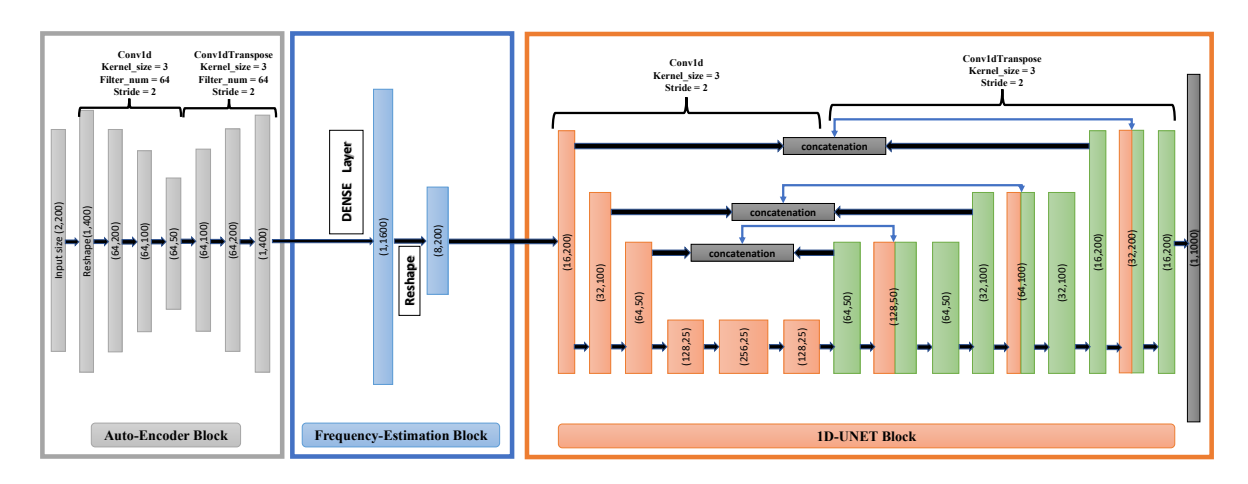


Fig. 3: The HRFreqNet Architecture

to generate multiple FRs. The output feature maps of the dense layer within this block have dimensions of  $1 \times BN$ . These feature maps undergo reshaping within the block to yield  $B \times N$ , representing B pseudo FRs. In Figure 3, we illustrate a sample signal with a length of 200, partitioned into real and imaginary parts in a 2-channel configuration. In the frequency estimation block, following the dense layer of size  $1 \times 1600$ , the output is reshaped to  $8 \times 200$ , where 8 denotes the number of pseudo FRs. Figure 4 showcases the frequency spectra learned from the weights of the frequency estimation block, unveiling the presence of 8 distinct Fourierlike transformations, each spanning the entire frequency range. Each of these transformations is capable of generating FRs for the original signal, thus providing a diverse set of frequency features for the subsequent U-net block to produce a highresolution FR.

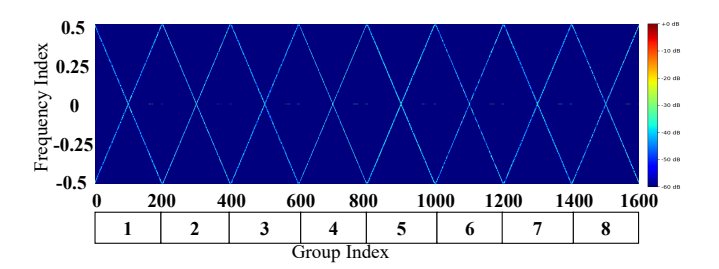


Fig. 4: Visualization of the frequency spectra learned by the Frequency Estimation block.

3) 1D UNET Module: The primary objective of the 1D U-Net module is to combine multiple frequency FR feature maps from the Frequency Estimation module into a high-resolution FR. This module adopts an encoder-decoder architecture: the encoder employs convolutional layers for hierarchical feature extraction, while the decoder utilizes transposed convolutional layers for feature map upsampling. Skip connections, established through concatenation, facilitate the integration of low-level and high-level features, promoting detailed frequency

analysis. The final convolutional layer produces a single-channel output with the shape of  $1 \times 1000$ , representing the high-resolution FR.

4) Training the proposed architecture: Our training dataset comprises  $3 \times 10^5$  noisy signals, with uniformly random generated signal-to-noise ratio (SNR) levels ranging from 0 to 15 dB. For validation, a separate set of  $3 \times 10^4$  noisy signals is used, with SNR levels following the same distribution. The loss in the 1D-UNet module denoted as  $L_2$ , is SSE loss between the final FR output of the model and the labeled FR. This  $L_2$  loss is combined with the loss in the autoencoder block, denoted as  $L_1$ . The overall loss utilized for training the entire model is defined as:

$$L_{\text{total}} = \lambda \times L_1 + L_2 \tag{7}$$

Here,  $L_{\text{total}}$  represents the cumulative training loss, and the hyperparameter  $\lambda$  is systematically tuned to a value of 2 through an iterative process to optimize model performance. The flow diagram of the proposed model is illustrated in Fig. 2 for better visualization.

# 

In this section, we will evaluate the performance of the proposed HRFreqNet model.

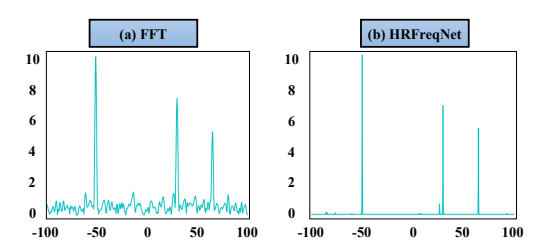


Fig. 5: Frequency Representation of the Signal (8) by (a) FFT, (b) HRFreqNet.

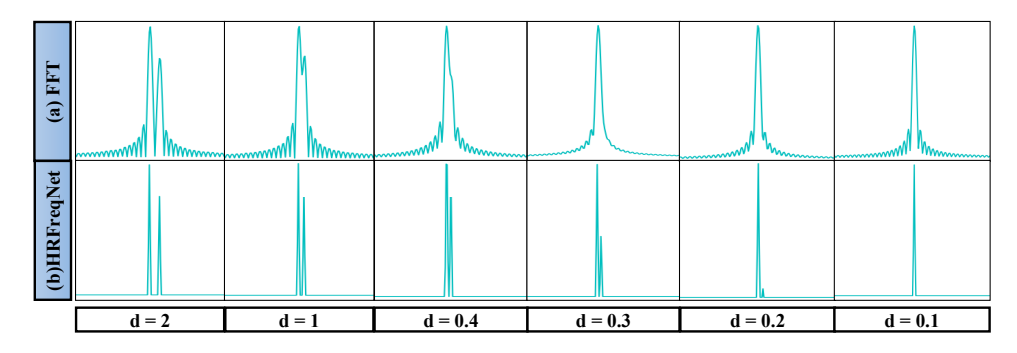


Fig. 6: Frequency Representation of the Signal (9) by (a) FFT, (b) HRFreqNet.

#### A. Simulation Validation

To illustrate the performance of the proposed approach, an example signal consisting of three frequency components is considered. The signal is given as follows:

$$s(t) = 10 \exp(j2\pi(-50)t) + 7 \exp(j2\pi 30t) + 5 \exp(j2\pi 65t)$$
(8)

In this experiment, the SNR was 10 dB, and the signal length is 200 with a sampling frequency of  $f_s$ =200. Figure 5a and 5b shows the FR of signal (8) for FFT and HRFreqNet respectively. The proposed model can generate a much sparser FR than the standard FFT.

### B. High-Resolution Frequency Representation

This section will analyze and compare the model's performance in terms of distinguishing closely related frequency points. To test this, we chose a noiseless signal with two frequency components, with a constant frequency difference. The sampling frequency and the duration are 200 Hz and 1 sec respectively. The generated FR had a dimension of  $1\times1000$  for both cases. The signal representation is given as,

$$s(t) = 10 \exp(j2\pi 10t) + 7 \exp(j2\pi (10+d)t)$$
 (9)

In Fig. 6, for d = 2, both FFT and HRFreqNet effectively distinguished two frequency components. However, as d decreased below 4, FFT gradually lost this capability, while HRFreqNet maintained clear separation. HRFreqNet could still distinguish the components even at d < 0.3, although amplitude identification slightly diminished. Notably, at d < 0.1, HRFreqNet also lost its ability to distinguish the two components. This highlights HRFreqNet's superior frequency resolution and low sidelobe levels compared to FFT.

# C. Range Profile generation in different SNR levels

Figure 7 shows the synthetically generated range profiles (RPs) from the proposed HRFreqNet model along with FT and the ML-based methods for the same signal under different SNR conditions varying from 20 dB to -10 dB. Important to note that, all the DL-based methods, as well as the standard FT, yield accurate RPs when applied to higher SNRs (20dB). The DL-based approaches especially CresFreq and HRFreqNet

were able to produce sparser RPs compared to other methods. But at lower SNR levels (0 or -10 dB), the DL-based methods, DeepFreq and CresFreq, performed really poorly. The RP generated by applying FT shows the frequency components in a noisy background. The proposed HRFreqNet can produce accurate RPs in a much cleaner background. This is because of the two-level noise suppression process from HRFreqNet, first from the auto-encoder module and second from the 1D-Unet module.

Overall, the proposed HRFreqNet model outperforms the other methods including FT in terms of noise suppression and frequency resolution at lower SNR conditions. This suggests that HRFreqNet could be used for applications where sparse radar RPs are required in a noisy environment, such as radar target recognition or object tracking.

# D. Range Profile generation in Real-world Scenario

In this section, we are showing the capability of HRFreqNet to generate RPs from real-world radar data. Figure 8 shows the RPs from walking and running. This data was collected from INRAS Radarbook2 FMCW radar with a duration of 1 second. The RPs generated from HRFreqNet are much cleaner. In the future, we will collect data from multiple targets at the same time to show the sparsity clearly in real-world scenarios.

## V. Conclusion

HRFreqNet, a novel deep learning architecture, excels at reconstructing precise frequency representations of complex multi-sinusoidal signals. The initial study shows the model's noise resilience and generalization capability in both synthetically generated and real-world datasets. It holds promise for RF-sensing-based target detection and tracking. The HRFreqNet model currently takes a particular length signal as input. In the future, we will upgrade or model in such a way that it is able to take the signal of any length. Also, we will do an extensive analysis in terms of noise suppression, sparsity calculation, and computational complexity for the proposed approach as well as comparisons with other DL-based approaches.

## ACKNOWLEDGMENT

The presented study was funded in part by the National Science Foundation (NSF) Awards #2047771.

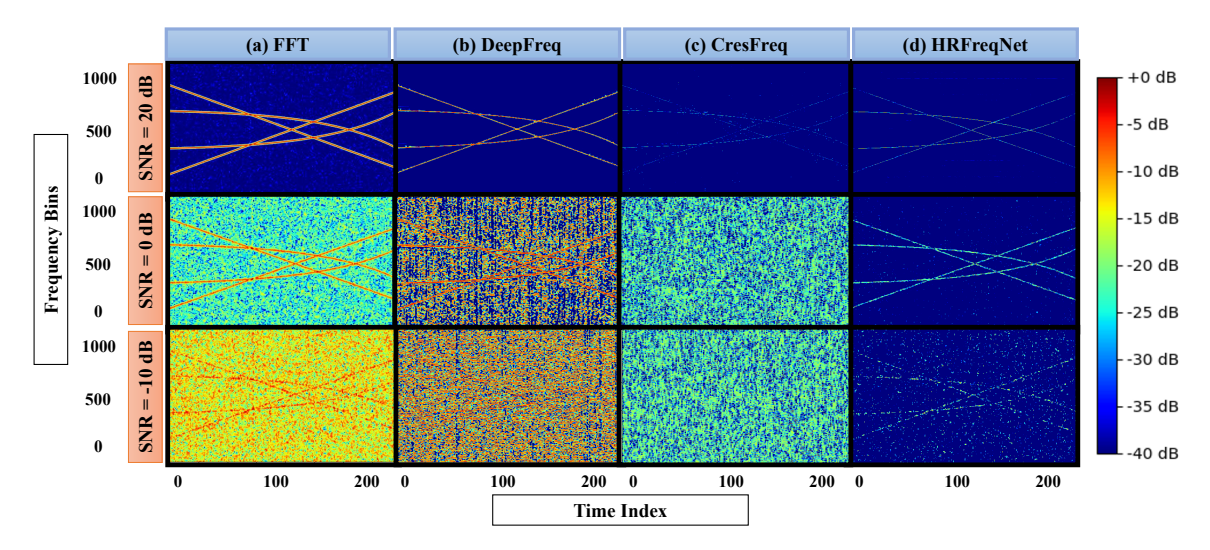


Fig. 7: Example of Range Profile in different SNR levels generated using (a) FFT, (b) DeepFreq, (c) CresFreq, (d) HRFreqNet.

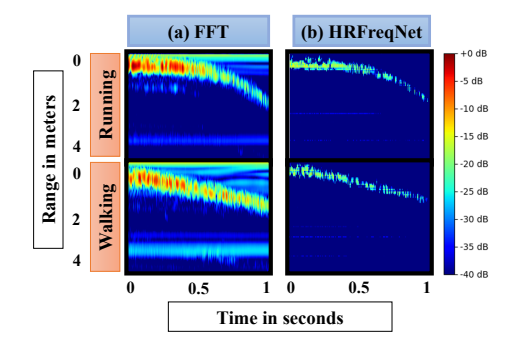


Fig. 8: Range Profile of walking and running generated from (a) FFT and (b) HRFreqNet.

## REFERENCES

- V. Chen and S. Qian, "Time-frequency transform vs. fourier transform for radar imaging," in *Proceedings of Third International Symposium on Time-Frequency and Time-Scale Analysis (TFTS-96)*, 1996, pp. 389–392.
- [2] A. Sadat and W. Mikhael, "Fast fourier transform for high speed ofdm wireless multimedia system," in *Proceedings of the 44th IEEE 2001 Midwest Symposium on Circuits and Systems. MWSCAS 2001 (Cat. No.01CH37257)*, vol. 2, 2001, pp. 938–942 vol.2.
- [3] D. S. Kim and E. Lee, "Estimation of zero-frequency noise power density in digital imaging," *IEEE Signal Processing Letters*, vol. 25, no. 11, pp. 1755–1759, 2018.
- [4] A. Klapuri, "Multiple fundamental frequency estimation based on harmonicity and spectral smoothness," *IEEE Transactions on Speech and Audio Processing*, vol. 11, no. 6, pp. 804–816, 2003.
- [5] X. Zhang, X. Han, J. Yin, and X.-l. Sheng, "Study on Doppler effects estimate in underwater acoustic communication," *Proceedings of Meetings on Acoustics*, vol. 19, no. 1, p. 070062, 06 2013.
- [6] A. M. Alam, M. Kurum, M. Ogut, and A. C. Gurbuz, "Microwave radiometer calibration using deep learning with reduced reference information and 2-d spectral features," *IEEE Journal of Selected Topics* in Applied Earth Observations and Remote Sensing, vol. 17, pp. 748– 765, 2024.
- [7] S. Biswas, B. Bartlett, J. E. Ball, and A. C. Gurbuz, "Classification of traffic signaling motion in automotive applications using fmcw radar," in 2023 IEEE Radar Conference (RadarConf23), 2023, pp. 1–6.
- [8] S. Biswas, C. O. Ayna, S. Z. Gurbuz, and A. C. Gurbuz, "Cv-sincnet: Learning complex sinc filters from raw radar data for computationally

- efficient human motion recognition," *IEEE Transactions on Radar Systems*, vol. 1, pp. 493–504, 2023.
- [9] T. Stadelmayer and A. Santra, "Data-driven radar processing using a parametric convolutional neural network for human activity classification," *IEEE Sensors Journal*, vol. 21, pp. 19529–19540, 2021.
- [10] S. Biswas, C. O. Ayna, S. Z. Gurbuz, and A. C. Gurbuz, "Complex sincnet for more interpretable radar based activity recognition," in 2023 IEEE Radar Conference (RadarConf23), 2023, pp. 1–6.
- [11] S. Gurbuz, Ed., Deep Neural Network Design for Radar Applications. London: IET, 2020.
- [12] E. Kurtoğlu, S. Biswas, A. C. Gurbuz, and S. Z. Gurbuz, "Boosting multi-target recognition performance with multi-input multi-output radar-based angular subspace projection and multi-view deep neural network," *IET Radar, Sonar & Navigation*, vol. 17, no. 7, pp. 1115–1128, 2023.
- [13] B. Debnath, I. A. Ebu, S. Biswas, A. C. Gurbuz, and J. E. Ball, "Fmcw radar range profile and micro-doppler signature fusion for improved traffic signaling motion classification," in *Proc. 2024 IEEE Radar Conference (RadarConf24)*, 2024.
- [14] A. Huizing, M. Heiligers, B. Dekker, J. de Wit, L. Cifola, and R. Harmanny, "Deep learning for classification of mini-uavs using micro-doppler spectrograms in cognitive radar," *IEEE Aerospace and Electronic Systems Magazine*, vol. 34, no. 11, pp. 46–56, 2019.
- [15] S. Z. Gurbuz and M. G. Amin, "Radar-based human-motion recognition with deep learning: Promising applications for indoor monitoring," *IEEE Signal Processing Magazine*, vol. 36, no. 4, pp. 16–28, 2019.
- [16] A. Dahal, S. Biswas, and A. C. Gurbuz, "Comparison between wifi-csi and radar-based human activity recognition," in *Proc.* 2024 IEEE Radar Conference (RadarConf24), 2024.
- [17] G. Hakobyan and B. Yang, "High-performance automotive radar: A review of signal processing algorithms and modulation schemes," *IEEE Signal Processing Magazine*, vol. 36, no. 5, pp. 32–44, 2019.
- [18] S. Biswas, J. E. Ball, and A. C. Gurbuz, "Radar-lidar fusion for classification of traffic signaling motion in automotive applications," in 2023 IEEE International Radar Conference (RADAR), 2023, pp. 1–5.
- [19] F. Fioranelli and J. L. Kernec, "Contactless radar sensing for health monitoring," in *Engineering and Technology for Healthcare*, 2021, pp. 29–59.
- [20] G. Izacard, S. Mohan, and C. Fernandez-Granda, "Data-driven estimation of sinusoid frequencies," in *Advances in Neural Information Processing Systems*, vol. 32. Curran Associates, Inc., 2019.
- [21] P. Pan, Y. Zhang, Z. Deng, and G. Wu, "Complex-valued frequency estimation network and its applications to superresolution of radar range profiles," *IEEE Transactions on Geoscience and Remote Sensing*, vol. 60, pp. 1–12, 2022.
- [22] I. Ilhan, A. C. Gurbuz, and O. Arikan, "Compressive sensing-based robust off-the-grid stretch processing," *IET Radar, Sonar & Navigation*, vol. 11, no. 11, pp. 1730–1735, 2017.